JOURNAL OF GEOPHYSICAL RESEARCH, VOL. 113, E06S05, doi:10.1029/2007JE002953, 2008

Soil sedimentology at Gusev Crater from Columbia Memorial Station to Winter Haven

Nathalie A. Cabrol,[1,2] Kenneth E. Herkenhoff,[3] Ronald Greeley,[4] Edmond A. Grin,[1,2] Christian Schröder,[5] Claude d'Uston,[6] Catherine Weitz,[7] R. Aileen Yingst,[8] Barbara A. Cohen,[9] Jeffrey Moore,[1] Amy Knudson,[4] Brenda Franklin,[10] Robert C. Anderson,[11] and Ron Li[11]

Received 11 June 2007; revised 26 October 2007; accepted 22 February 2008; published 17 May 2008.

[1] A total of 3140 individual particles were examined in 31 soils along Spirit's traverse. Their size, shape, and texture were quantified and classified. They represent a unique record of 3 years of sedimentologic exploration from landing to sol 1085 covering the Plains Unit to Winter Haven where Spirit spent the Martian winter of 2006. Samples in the Plains Unit and Columbia Hills appear as reflecting contrasting textural domains. One is heterogeneous, with a continuum of angular-to-round particles of fine sand to pebble sizes that are generally dust covered and locally cemented in place. The second shows the effect of a dominant and ongoing dynamic aeolian process that redistributes a uniform population of medium-size sand. The texture of particles observed in the samples at Gusev Crater results from volcanic, aeolian, impact, and water-related processes.

Citation: Cabrol, N. A., et al. (2008), Soil sedimentology at Gusev Crater from Columbia Memorial Station to Winter Haven, *J. Geophys. Res.*, *113*, E06S05, doi:10.1029/2007JE002953.

1. Introduction

[2] Since landing in Gusev Crater in January 2004, Spirit has documented a diversity of bed forms including dunes, ripples, drifts [*Greeley et al.*, 2004, 2006; *Herkenhoff et al.*, 2006], and unstructured soils [*Cabrol et al.*, 2006]. Their mineralogy and chemistry [*Gellert et al.*, 2004; *Morris et al.*, 2004; *Christensen et al.*, 2004; *Yen et al.*, 2005] show a trend from basaltic soils in the Plains Unit [*McSween et al.*, 2004] with evidence for limited water alteration [*Haskin et al.*, 2005] to soils increasingly rich in sulfate locally in the Columbia Hills [*Gellert et al.*, 2006; *Morris et al.*, 2006; *Ming et al.*, 2006; *Wang et al.*, 2006]. While these analyses provide information about the nature of the soils, the size and shape of individual particles constrain their formation and the various processes affecting their evolution.

[3] Here, we present an example of quantitative techniques applied to the Microscopic Imager (MI) and the results of analyses performed on all undisturbed soils surveyed by Spirit's from landing at the Columbia Memorial Station to Winter Haven (sol 1085) (see Figure 1). This quantitative classification of soils along the traverse at Gusev Crater extends and completes the vision of soil sedimentology obtained from previous local and regional analyses along Spirit's traverse [*Herkenhoff et al.*, 2004, 2006; *Cabrol et al.*, 2006, 2007; *Cabrol and Grin*, 2006; K. E. Herkenhoff et al., Overview of the Microscopic Imager results at the Opportunity landing site, submitted to *Journal of Geophysical Research*, 2008]. Characteristics such as particle-size distribution, elongation, roundness/angularity, texture, sorting, and morphology as observed in the sample were examined and quantified. These characteristics are particularly important as indicators of soil dynamics and provide clues to understanding whether and how particles have been mobilized.

[4] A systematic quantification of Martian soil sedimentology is critical for the understanding of geologic processes and their evolution on Mars through time and this paper represents a first attempt in that direction; These results can also be used to more precisely model past and present erosional and depositional activity on Mars, in particular as related to aeolian (e.g., wind strength, dust deposition, particle transport, erosion, saltation) [e.g., *Greeley et al.*, 2006, 2008] and aqueous processes, whether at large scale

[1]Space Science and Astrobiology Division, NASA Ames Research Center, Moffett Field, California, USA.
[2]SETI Institute Carl Sagan Center, Mountain View, California, USA.
[3]U.S. Geological Survey, Flagstaff, Arizona, USA.
[4]Department of Geological Sciences, Arizona State University, Tempe, Arizona, USA.
[5]Institute Inorganic and Analytical Chemistry, Johannes Gutenberg-University, Mainz, Germany.
[6]Centre d'Etude Spatiale des Rayonnements 9, Toulouse, France.
[7]Planetary Science Institute, Tucson, Arizona, USA.
[8]Natural and Applied Sciences, University of Wisconsin Green Bay, Green Bay, Wisconsin, USA.
[9]Department of Earth and Planetary Sciences, University of New Mexico, Albuquerque, New Mexico, USA.
[10]Jet Propulsion Laboratory, Pasadena, California, USA.
[11]CEEGS/Center for Mapping, Ohio State University, Columbus, Ohio, USA.

0148-0227/08/2007JE002953$09.00

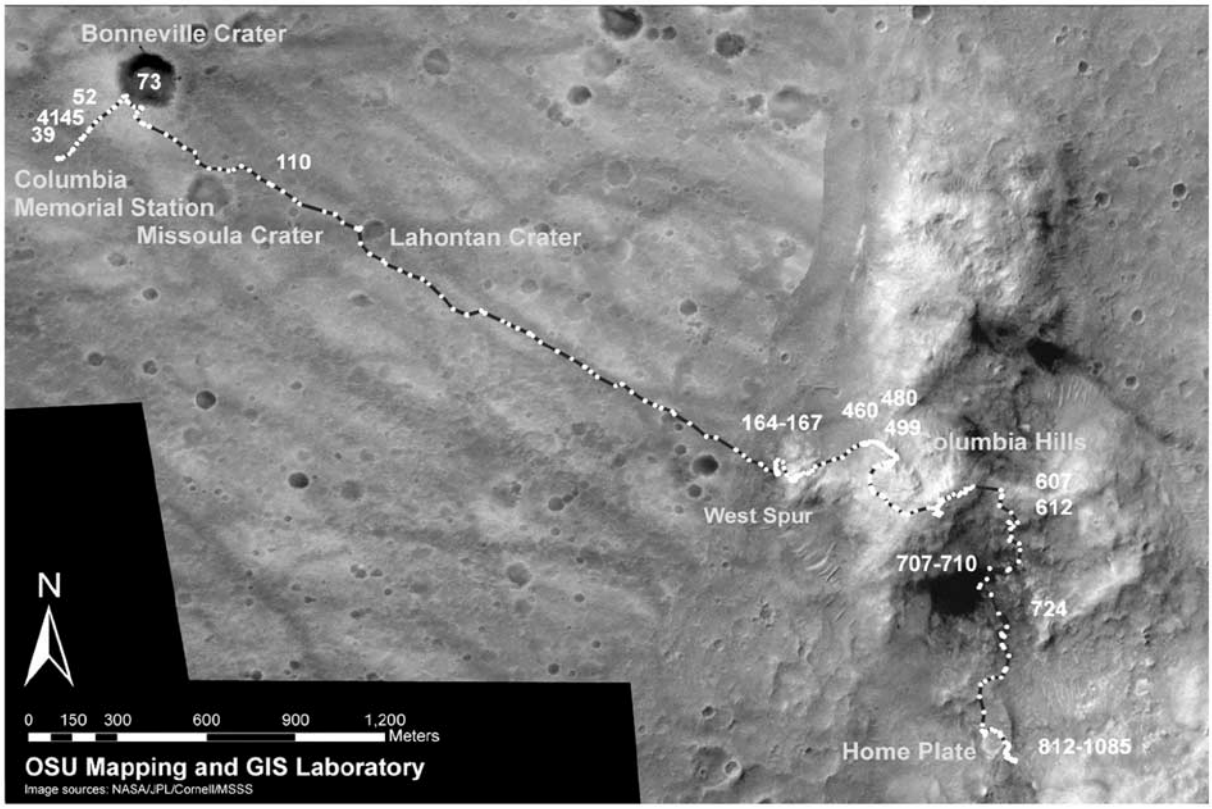

Figure 1. Spirit's traverse between the Columbia Memorial Station and Winter Haven. White dots are Spirit stops on the traverse. Sols marked on the map show where MI images were surveyed. A total of 13 soils were analyzed at Winter Haven between sols 812 and 1085.

(erosion capacity, sediment load, and transport in streams) or at microscale (particle cementation).

2. Analytical Method

[5] Textural characteristics were analyzed on 3140 particles over 31 undisturbed soils; an average of 100 particles were counted per MI image. The MI has a pixel scale of 31 μm allowing the identification of individual particles as small as 100 μm across [*Herkenhoff et al.*, 2004]. Limitations and constraints on soil measurement have been described in previous studies at Gusev and Meridiani [e.g., *Herkenhoff et al.*, 2004, 2006, also submitted manuscript, 2008; *Cabrol et al.*, 2005, 2006; *Sullivan et al.*, 2005, R. Sullivan et al., Active saltating fraction at Gusev Crater, focusing on El Dorado, submitted to *Journal of Geophysical Research*, 2008; *Weitz et al.*, 2006] and relate to the observer's ability to clearly identify the particle's boundary. Although measurement errors cannot be completely avoided, steps can be taken to significantly decrease them. To that end, we did not measure particles less than 100 μm in size, partly buried or hidden particles, and did not analyze images taken under poor lighting conditions.

[6] Representative areas in each MI image were selected for statistical data collection including particles' long (L) and short (w) axes with an average deviation of ±1 pixel, from which elongation ($q = w/L$) was inferred (Figures 2a and 2b). Depending on the type of sample, especially when the sample is homogeneous in size like that of the El Dorado dune, it is not necessary to count all grains in the entire image. A subset of the image can be chosen and the result normalized to the total surface area of the image. When samples are heterogeneous (e.g., a mixture of small, large, rounded, and angular grains), it is important to select an area of the image that reflects the diversity both in sizes and relative proportion of every type of grains in the entire image. If this is not possible, then all grains are measured.

[7] Particle perimeter (p) and area (A) were obtained from pixel density analysis (PDA). PDA was performed using an image processing application (NIH) on a subset of 136 particles representative of the surveyed soils. The boundary of the particles was delineated manually on the digital MI images; the measurement tool of the application was then used to follow the delineated contours; finally, the surface area and perimeter were calculated automatically by the software. The area (A) was calculated as the number of MI pixels that form the visible face of a particle, and the perimeter (p) as the number of pixels of the particle that touch the image background (Figure 2c).

[8] Roundness (Rn) was inferred from the relationship between the perimeter and the area, such as $Rn = 4\pi A/p^2$ [e.g., *Janoo*, 1998]. This equation differs from that of circularity (particle perimeter/perimeter of circle having same area as particle) which measures the closeness of a particle to a perfect circle. Rn has a squared term in the numerator and denominator in order to sensitize the param-

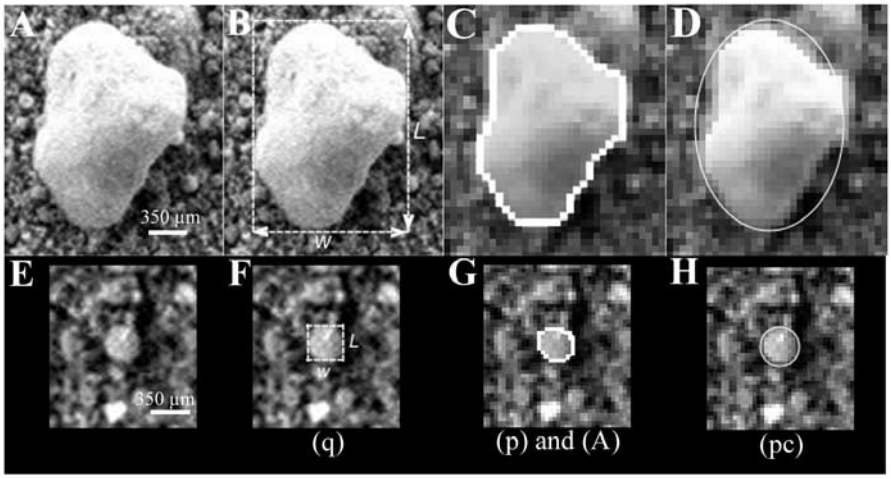

Figure 2. Particle measurement. Textural characteristics of (a–d) a granule and (e–h) a medium sand showing the increased complexity of measurement with decreasing particle size. Figures 2b and 2f show estimation of the long and short axes, from which elongation (q) is inferred; Figures 2c and 2g show manual delineation of the particle's perimeter (white contour line). The surface area is calculated as the number of pixels of the visible face of the particle, which includes the gray area and the delineated perimeter; Figures 2d and 2h show best fit of an ellipse to the particle.

eter to subtle variations in the area-perimeter relationship. As a result, it allows expression of the shape of a particle more in terms of roundness/angularity rather than circularity alone. Our survey showed consistent morphological observations for all classes of shapes defined by *Rn* and for all studied particle sizes as shown in section 4.0. They define families of particles along the traverse. As a result, we classified the particles in six categories: very round (*Rn* = 1–0.95); round (0.95–0.90); subround (0.90–0.85); subangular (0.85–0.80); angular (0.80–0.70); very angular ($\leq$0.70).

[9] Roughness (*r*) expresses how smooth or textured a particle surface is. It is defined as $r = pc/p$, where *pc* is the convex perimeter and *p* is the perimeter. The convex perimeter is obtained by manually fitting an ellipse to the contour of the particle (Figure 2d). For a perfectly smooth particle, $pc = 1.00$. Increasing roughness is shown by decreasing index values.

[10] Biases resulting from these techniques have been studied for terrestrial particles and aggregates [e.g., *Podczeck*, 1997; *Janoo*, 1998; *Alshibli and Alsaleh*, 2004; *Seelos and Sirocko*, 2005; *Uthus et al.*, 2005] and relate to the resolution of the image and the size of the particle. Perimeter and area evaluations are more sensitive to variations in texture at high resolution and to changes in angularity at low resolution.

3. Textural Characteristics

[11] The undisturbed soils surveyed in this study are bed forms (ripples, drifts, dunes) and composite soils, which are made of a mixture of materials. Unstructured soils composed mostly of particles below the MI resolution described by *Herkenhoff et al.* [2004] and *Cabrol et al.* [2006] require other analytical techniques and are not discussed here.

3.1. Particle-Size Distribution and Sorting

[12] Highly reworked fine-to-medium sand-blanketing units are dominated by particles averaging 270 μm in size (Figure 3), which forms the base of most ripples, drifts, dunes, and composite soils sampled at the Columbia Hills, including West Spur, Husband Hill, Inner Basin, and Winter Haven. While the bulk grain size is comparable among various bed forms, differences in particle-size frequency distributions separate them (Figure 4). They show specific mixings that may be related to variations in sediment sources (e.g., nature and resistance to erosion of parent material), soils dynamics (e.g., mass movement), and/or local to regional physical factors associated with the transport and deposition agents (e.g., wind direction, velocity, competency).

[13] The particle size–frequency distribution of ripple samples is at least bimodal. One peak is centered on medium sand (290 μm) and the other on coarse sand (540 μm), whereas in the Winter Haven region the coarser population is made of larger ($\sim$2 mm) grains (Figure 4d). Bimodality is consistent with either two sources of sediment or various processes affecting single source sediment.

[14] The drifts have similar sorting on average compared to ripples (variance $\sigma^2 = 0.01$ versus 0.02) but with only one main population centered at 270 μm, which corresponds to the smaller fraction observed in ripples.

[15] El Dorado, in the Inner Basin, was the only dune field surveyed in Inner Basin (Figure 4f). It has an identical distribution, similar peak at 270 μm, and comparable particle density as the drifts, but has the best sorting among all samples ($\sigma^2 = 0.005$). Sorting and shape are consistent with aeolian processes, which tends to continuously winnow away finer particles. Moreover, a minimal amount of dust particulates is observed on the grains or in the intergranular space suggesting current wind activity on the

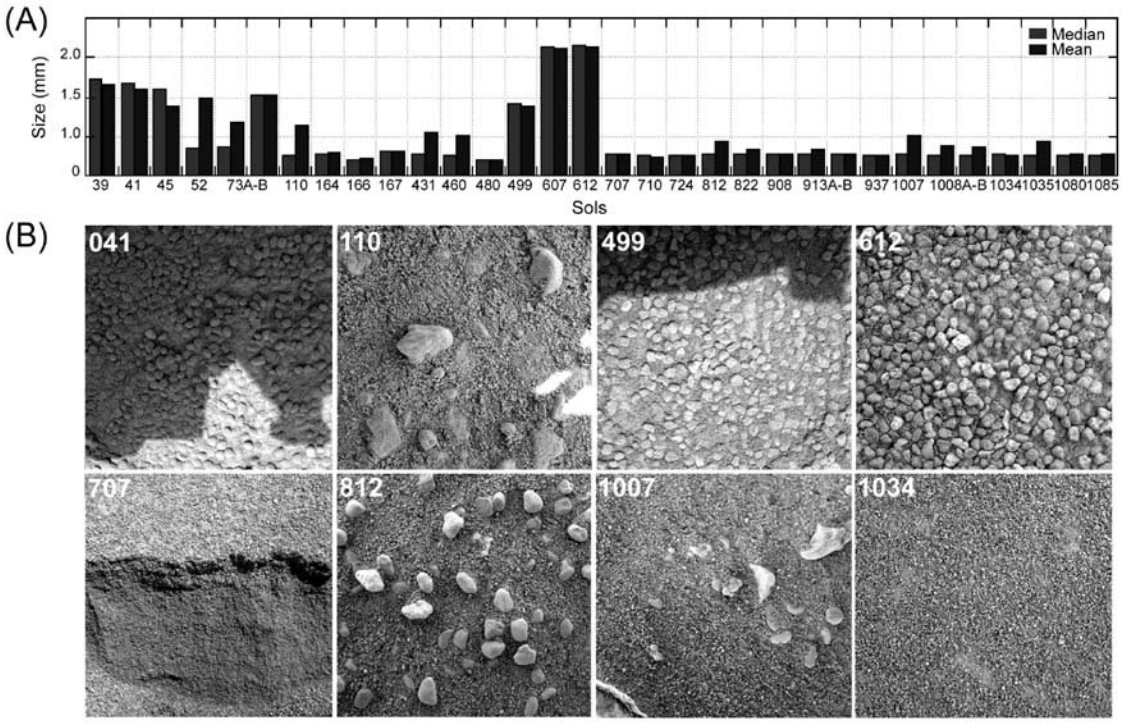

Figure 3. (a) Evolution of mean and median particle sizes along Spirit's traverse showing two distinct textural domains in the Plains Unit (sols 1–156) and the Columbia Hills (after sol 156). The "A" or "B" index attached to some sol numbers indicates that for the same sol two images of two different soil samples were analyzed. (b) MI images of representative soil types, particle textures, and shapes at Gusev. Each MI frame is 3.2 cm across. Sol numbers are indicated in the top left of the image; sol 041, ripple in the Plains Unit, 2M130001239; sol 110, composite soil in the Plains Unit, 2M136126236; sols 499 and 612, angular granules in the Columbia Hills, 2M170661212 and 2M180692664; sol 707, El Dorado dune, Inner Basin, 2M189124003; sol 812, medium sand and rounded granules in Inner Basin, 2M198449160; sols 1007 and 1034, medium sand, rounded granules, and angular clasts at Winter Haven, 2M215762509 and 2M218159020.

dunes, which was confirmed by observations of surface albedo and color changes on El Dorado during last Martian winter.

[16] Composite soils are bimodal to multimodal (e.g., Figures 4g and 4h). Their composition results from the mixing of particles of wide size range including fine sand (100 μm) to granule and pebble-size material (2–13 mm). One of their dominant populations is made of 250–270 μm, the same type of material observed in bed forms, consistent with the hypothesis of drift material passing over local and larger material (e.g., rock fragments, ejecta material, and granules).

[17] Results on the samples of the Plains Unit contrasts with that of the Columbia Hills. In one case (Figure 4c), the particle size distribution of a ripple in the Plains Unit (sol 045) appears similar to that of a composite soil in Husband Hill (sol 499,Figure 4h). While their sizes are comparable, the particles of sol 045 are rounded and dusty whereas those of Husband Hill are angular to very angular and mostly dust free, likely showing different origins, distinct exposition to erosion, different dynamics, distance from source, and/or transportation time. This example underscores the limitation of one approach only and the necessity of combining particle size distribution with other classifiers, such as shape, which are detailed in the following sections.

[18] By contrast to the Columbia Hills samples, medium sand is a minor component of the ripples and drifts as seen on sols 039, 041, 045, 052, and 073 (Figures 4a–4c). The fine-to-medium sand distribution is truncated in most histograms. This suggests a large dispersion of particle populations representing distinct origins and/or a variety of processes that moved specific size populations over time. It can also be an artifact of the sample limitation.

[19] Ripples have bimodal distributions similar to those observed in the Columbia Hills, but dominant populations are reversed in the existing samples. Very coarse sand to very fine granules (1–2 mm) dominate their composition with peak populations at 1.1 mm. Granules are characterized by a substantial dust cover as well as thick dust packing in intergranular spaces. Some have thin deposits consistent with cemented material indicating that those particles are not currently active and have been maintained in place (fossilized) for a significant period of time.

[20] Serpent, the drift analyzed on sols 73–74, has coarser grains on average. It is armored with a dominant population of 1.19–1.41 mm grains. Once scuffed, the core of the drift showed a population of smaller, medium-size, sand as well as particles below resolution. Serpent's armor of large grains is covered in dust. As a result of the scuff, some of the top large grains fell and accumulated in the

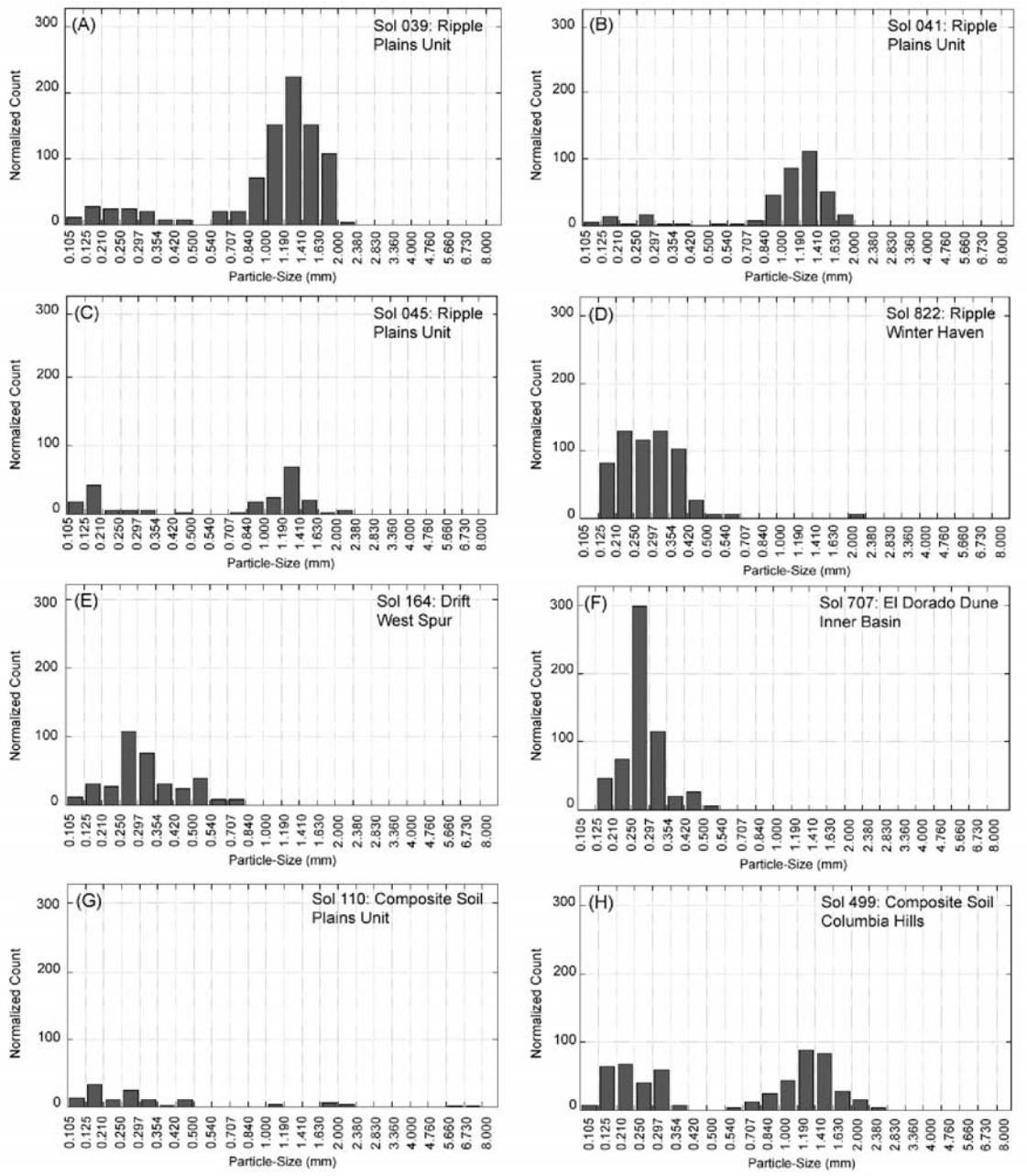

Figure 4. Histograms representative of soil types in the regions traversed by Spirit. Particle counts (y) are normalized to the entire MI surface area for direct comparison of results between histograms.

scuff area. Those grains were completely clean, most likely having lost their dust cover as they fell. This shows a weak bond between sand and dust grains in the sample. Considering the large amount of dust covering the drift, it appears that while it is easily removed, dust is probably replaced even faster on these grains. Another conclusion suggested by this observation is that Serpent is unlikely to be currently active.

[21] Elemental and mineralogical compositions show that the parent rock of bed forms in the Plains Unit is basaltic [*McSween et al.*, 2004]. Mineralogy and composition of the granules in the ripples reveal abundant magnetite compared to surrounding soils. Concentration of bromine was found and is best explained by limited water-mediated chemical activity associated with current diurnal and/or climatic cycles of condensation [*Yen et al.*, 2005] favoring cementation processes.

[22] The composite soil analyzed in the Plains Unit (sol 110, Figure 4g) suggests the juxtaposition of particle populations and processes. Its distribution is multimodal, truncated, and poorly sorted ($\sigma^2 = 1.67$). It is dominated by grains below resolution, accompanied by a small number of fine-to-coarse grains, granules, and angular to subrounded pebbles (e.g., ejecta fragment, rock debris). Pebbles and granules are covered by grains and aggregates of smaller dimension consistent with saltation (see also Sullivan et al.,

Table 1. Summary of Particle Sizes Per Region and Type

Soil Type	Sol	Particle Median Size, mm	Particle Mean Size, mm
Ripples			
Plain Unit	39, 41, 45, 73, 74	1.13	0.96
Winter Haven	822, 913, 1085	0.27	0.27
Drifts			
West Spur	164, 166, 167	0.28	0.29
Columbia Hills	480	0.25/1.64[a]	0.27/0.92[a]
Inner Basin	607, 612	0.27	
Winter Haven	937		
Dunes			
Inner Basin	707, 710	0.27	0.27
Composite Soils			
Plains Unit	110	0.25	0.64
Columbia Hills	431, 460, 499	0.28	0.56
Winter Haven	812, 1007, 1008	0.26	0.26

[a]Target Cliffhanger has a clear bimodal distribution with one peak centered on medium sand and the other one on very coarse sand. Median and mean values for the smaller grain fraction/values for both populations are given. When the coarser fraction is extracted, the distribution exhibits the same statistical attributes as many of the other soils at Gusev, suggesting the presence of a mixture of global sand and that of a material of different origin (see text).

submitted manuscript, 2008). Table 1 summarizes the size characteristics for all regions. Figure 5 summarizes the particle size distribution (normalized count) for all soil samples along Spirit's traverse, and Figure 6 shows their elongation.

3.2. Particle Shape

[23] The ripples of the Plains Unit have subrounded to rounded (average Rn = 0.86) and elongated (q = 0.78) particles compared to the elongation of the average sand fraction (q = 0.93) observed in other samples (Figure 6). This combination of roundness and elongation is (so far) unique along the traverse. It is consistent with aeolian processes, but other processes, including water, cannot be ruled out. The nature of the parent material of the clastic sediment (e.g., minerals producing elongated grains) may also have played a role.

[24] In the Columbia Hills, most of the grains forming the ripples, drifts, dunes, and composite soils have a roundness index ranging from round to subround (Rn = 0.90–0.80). However, isolated 420–460 μm particles stand out as spherical and have a roundness index of 0.95–1. Their frequency has been increasing since Spirit entered Inner Basin. Their abundance was measured as a percentage i.e., number of spherical particles/total number of particles normalized per 1024 mm^2 (the surface area observed by the MI at best focus). The first occurrence of spherical particles was noted at West Spur (1% on sol 164), then in Inner Basin at El Dorado (11% on sol 707) and Winter Haven (11% on sol 937 and 16% on sol 1034).

[25] The origin of these tiny spheres is unclear. Their shape is consistent with long-term erosion and/or short distance traveled by particles already very rounded to start with. Considering the most likely processes in the regional context, impact cratering and volcanic activity are known to generate spherules, i.e., glass beads, such as those observed in abundance in the lunar regolith [e.g., *Roedder and Weiblen*, 1973; *Heiken et al.*, 1991].

[26] Both impact cratering and volcanic activity also produce lapilli. Larger ($\geq$2 mm) spherical grains thought to be lapilli associated with an ancient hydrovolcanic event [*Rice et al.*, 2007; *Ennis et al.*, 2007; *Squyres et al.*, 2007] have been documented in the Home Plate area (e.g., Low Barnhill and Madeline English outcrops, sols 750 and 1168) and occur both detached from and included in rocks. Their erosion could provide a source for the microspherules.

[27] Another potential source could be the spherical grains (350–680 μm) observed in layered rocks such as Posey (sol 753) at Home Plate. They are embedded within a layered matrix composed of grains below resolution and other larger granular material (Figure 7). Their size is identical to that of the microspherules observed detached in the soil. Their erosion from rocks and outcrops and the location of their source area could explain their increased number as Spirit approached Home Plate.

[28] While small according to sedimentological classification, the size of these spherules does not prevent them from being lapilli (i.e., $\sim$50 μm lapilli have been observed in terrestrial rocks). Moreover, *Wilson and Head* [2007] have shown that on Mars lapilli could be on average

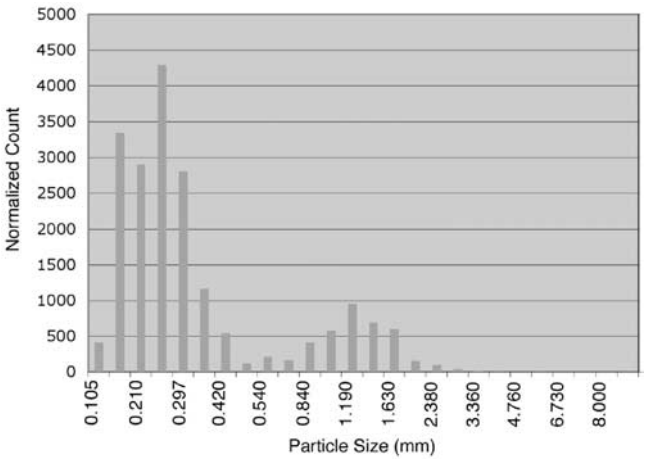

Figure 5. Statistical distribution of the normalized count of particles for all soil samples along Spirit's traverse. The normalized count represents a total of 19,510 particles. Fine to medium sand dominate; a second peak is centered on coarse sand. The scale of the chart does not allow visualization of a third minor peak centered on gravel and small pebbles (e.g., sol 110, Figure 4).

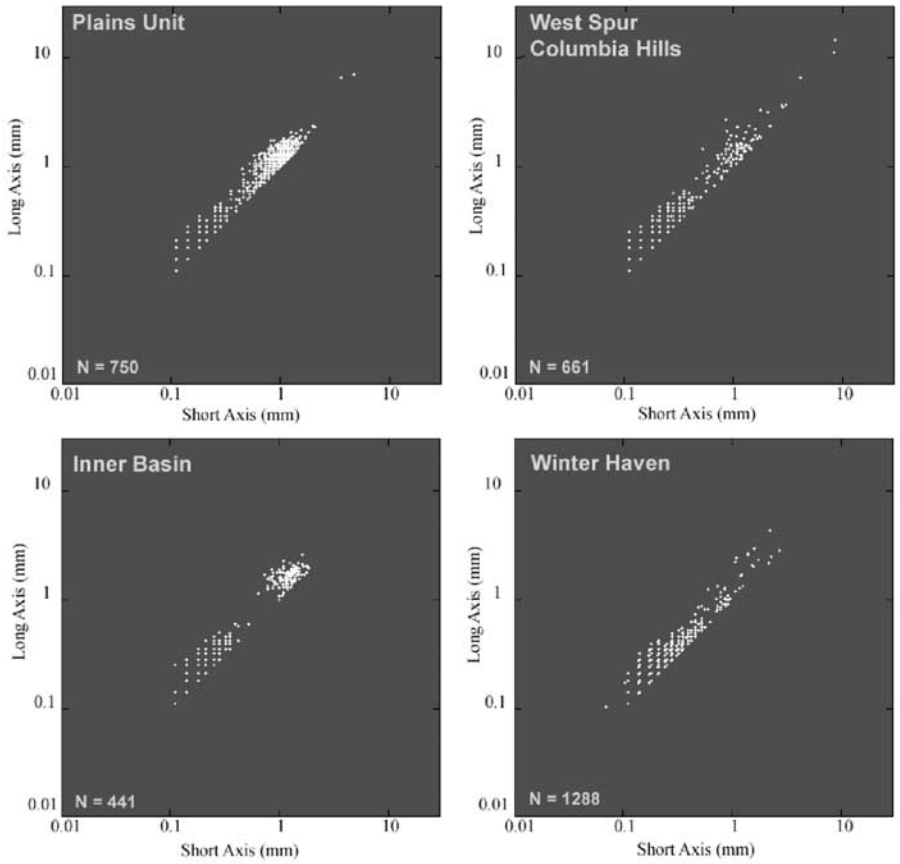

Figure 6. Particle elongation (q) along Spirit's traverse. The index ranges from 0 to 1. Deviation from (q) = 1 indicates elongation. For Winter Haven, the number of particles measured is larger than for the other regions, but many have similar dimensions and are characterized by only one point on the graph.

significantly smaller than on Earth. They can be formed either in volcanic base or impact surges but the abundance of local scoria, vesicular basalts, pumice-textured rocks, and ash-size material supports a volcanic origin [*Rice et al.*, 2006; *Squyres et al.*, 2007].

[29] Overall, a substantial fraction of soil particles along the traverse are rounded (Figure 8), suggesting an intense reworking process and/or distant sources for the clastic sediments, unless particles are rounded to start with, as discussed above. The largest round particle observed along the traverse is ~4 mm in size (granule). Soils targets on sols 499 (Doubloon) and 612 (Cliffhanger) on Husband Hill are two exceptions, with large, subangular to very angular granules (Rn = 0.81–0.70) suggesting less reworking and/or shorter distance from their sources. For Doubloon, this textural difference is correlated with the only ilmenite signature detected with the Mössbauer in soil targets so far. The neighboring rocks all contain abundant ilmenite suggesting that the soil composition is a mixture of local rock fragments and a regional/global soil component.

[30] Only a limited number of small grains were found in the existing samples to be angular, the smaller one being a medium sand ~350 μm in size. No smaller angular particle has been detected so far, which could also be the result of the limited number of samples, or an indication of instrument and method constraints (e.g., limit of MI perception of angularity). Image resolution and quality impact the results

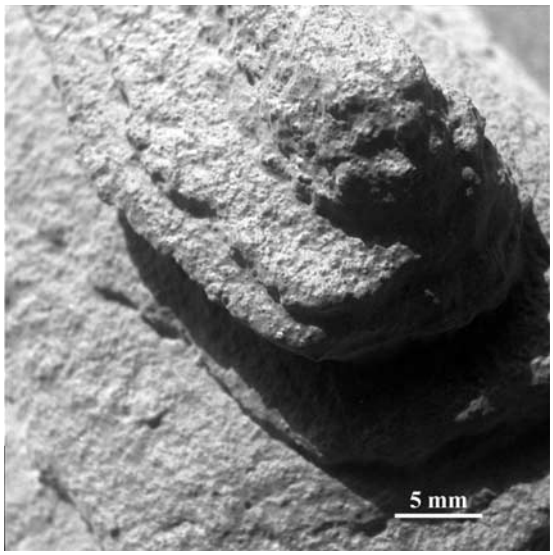

Figure 7. Rock Posey, Home Plate (sol 753). This layered rock includes tiny spherules that give a granular texture to the surface and material below resolution suggested to be ash. Spherules eroding away from the rocks such as Posey could be the origin of the increased number of spherical particles found in the soils since Inner Basin.

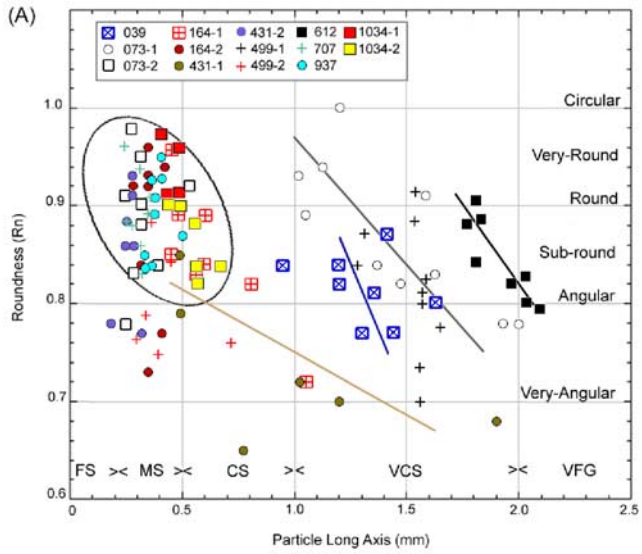

Figure 8. Roundness index for 136 particles representative of the soils traversed by Spirit. Indexes "1" or "2" next to a sol number indicate that particles of the two dominant populations in one MI image were analyzed. Trends in shape versus size are shown by straight lines and are fairly consistent throughout the traverse except for ejecta material (brown line) which shows increased angularity with size in some cases. The cluster of small particles indicates that regardless of the region, small particles appear rounded to well rounded at Gusev. This result could be explained as a physical reality of particles being transported and eroded for extended periods of time. It could be also an artifact of resolution, since angularity is harder to perceive with smaller particle size. The smaller angular particle observed so far at Gusev in this survey is 350 μm.

of particle identification. Figure 9 shows how roundness and angularity are represented in the four classes of grain sizes surveyed. It is interesting to note the opposite trends between the histogram of distribution for the smallest (200–400 μm) and largest (1800–3200 μm) particle classes. A majority of small grains appear very round to round; their frequency declines as angularity increases. Conversely, the large grains have increasing frequency toward angularity. These opposite trends are consistent with a resolution effect in the interpretation, as limitation in resolution tends to smooth the edge of small particles while smaller edges are more visible on large grains and easier to measure. This is a recognized and quantified effect of digital image analyses [e.g., *Podczeck*, 1997; *Janoo*, 1998; *Alshibli and Alsaleh*, 2004; *Seelos and Sirocko*, 2005; *Uthus et al.*, 2005].

[31] Characterization of sand using digital images have demonstrated that measurement accuracy is in direct relationship with the dimension of the grain and can be approximated as Accuracy = 1 − Error/dimension [e.g., *Wagner et al.*, 2003]. The average measurement error with MI being estimated at ±1 pixel (31 μm), 85% accuracy should be reached with grains of 200 μm, 95% at 700 μm, and 99% just under 4 mm. The accuracy falls to 38% for grains of 100 μm (smallest grains measured with MI). With an error of ±2 pixels, accuracy is 85% at 400 μm and 99% at 8 mm. The sharp decrease of frequency with angularity for the 200–400 μm particles as shown in Figure 9 appears inconsistent with an accuracy level of ±1 pixel for such small particles. On the other hand, a ±2 pixel measurement error would provide the same accuracy (85%) for particles 400 μm in size, consistent with the more homogeneous results shown in the Figure 9 histogram for the population of grains between 400 and 800 μm. This suggests that some level of optimization might be reached between particle size and instrument resolution and that a greater level of confidence can be attributed to measurement results starting 400 μm. It also confirms that measurement error increases as particle size decreases and is unlikely to be constant throughout the analysis of an heterogeneous sample.

4. Sedimentological Classification of Particles Along the Traverse

[32] Combined, sizes and shapes provide the tools to initiate a sedimentological classification for the surveyed soils along the traverse so far (Figure 10); their quantification gives a promising method for the identification of families of Martian particles based on shape coefficients that are now being accessed through microscopic imagery, such as (*Rn*, *q*, and *r*). The great diversity of particle textural signatures within what is still a limited sample size hints at the complex geological history of the crater basin and supports the existence of volcanic, aeolian, and aqueous processes at Gusev through time.

[33] When compared, the Columbia Hills and Plains Unit samples can be characterized by two specific textural classifications (Figure 11). The first one is homogeneous and shows the effect of one dominant, dynamic, and ongoing process (aeolian) that redistributes a uniform pop-

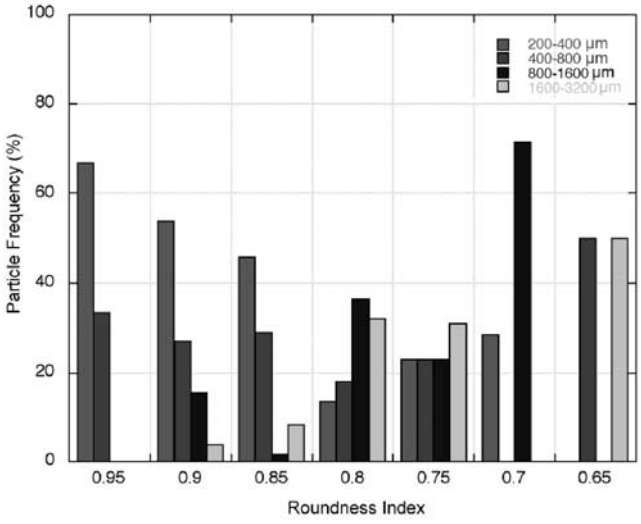

Figure 9. Frequency of particles for given classes of size as a function of shape. The opposite trend between the smallest and largest size classes suggests interpretation limitations related to instrument resolution (see text for discussion).

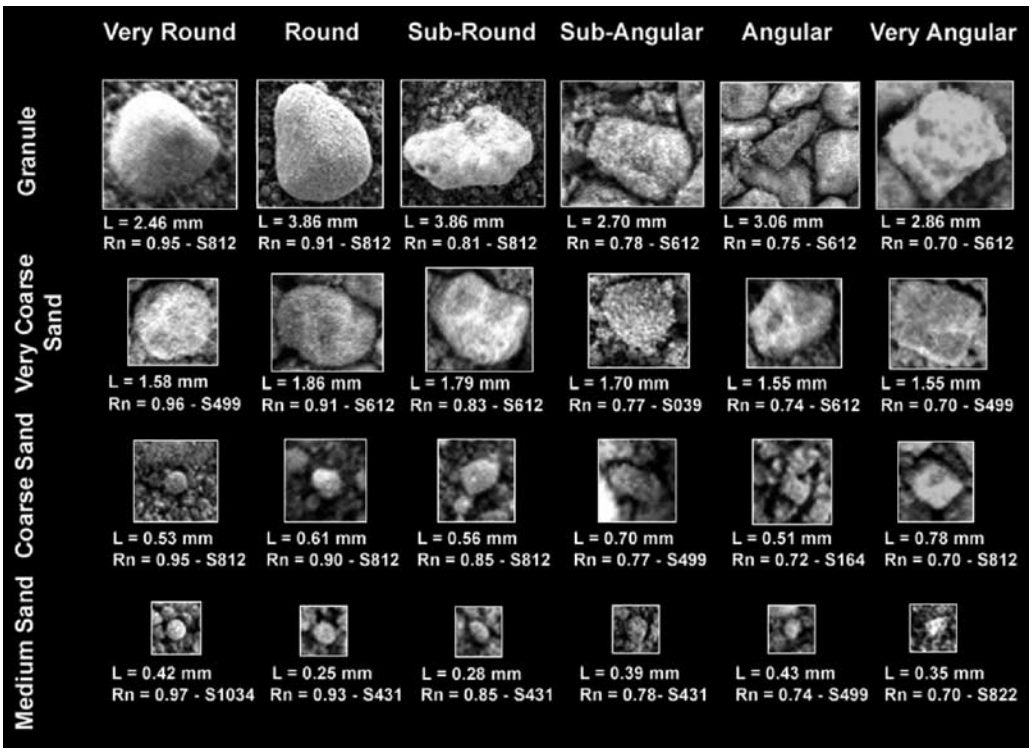

Figure 10. Quantitative classification of particle types obtained from ranges of sizes and shapes in Gusev soils. *L* is the long axis of the particle; *Rn* is the roundness index. *S* indicates the sol number.

ulation of rounded, small particles that have been shaped and transported over long periods of time and/or were very rounded to start with; the other is highly heterogeneous and is a collection of shapes (round, elongated, angular), sizes (fine sand to pebbles), and sorting. Unlike the Columbia Hills Formation (CHF), there is no evidence for any significant ongoing redistribution of material in the samples from the Plains Unit at MI resolution, indicating that whatever process was involved in these soils emplacement is not active anymore.

[34] Finally, compared to Meridiani [*Sullivan et al.*, 2005; *Weitz et al.*, 2006, Herkenhoff et al., submitted manuscript, 2008] Gusev soils are very distinct due to the lack of a population of 1–4 mm diameter hematite-rich spherules like those at the site investigated by the Opportunity rover [*Soderblom et al.*, 2004]. The spherules form a lag surface on most Meridiani soils with basalt sand and dust dominating the soils a few centimeters beneath this lag. Ripples at Meridiani have a surface armor of spherules yet the sizes and shapes of the spherules on the ripples (1.3–1.7 mm) is similar to the larger grains that armor the Plains Unit ripples at Gusev. The similar size grains on aeolian ripples at two landing sites located on opposite sites of Mars suggests that winds along the plains that form Martian ripples are similar in strength and favor transport of grains between 1 and 2 mm.

5. Conclusion

[35] Spirit has acquired over 107,200 images as of February 2008 and recorded a wealth of data on a diversity of soils and rocks since landing. While spectrometers are critical in determining composition, the MI generates information about micromorphology, sedimentology, depositional and postdepositional processes, and physical properties. From the Plains Unit to the Columbia Hills, classifications of rocks and soils based on Pancam multispectral images, Miniature-Thermal Emission Spectrometer (Mini-TES) spectra, and the Alpha Particle X-Ray Spectrometer (APXS) and Mössbauer (MB) data were established. They were named after the rock or outcrop where they were identified for the first time [e.g., *Squyres et al.*, 2006; *Dreibus et al.*, 2006; *Blaney et al.*, 2006]. While these combined data sets give important clues about the origin of the rocks and soils they can fall short of providing an explanation as to why rocks of similar spectral and compositional signatures have sometimes distinct morphologies and what could be the mechanical and physical processes that shaped them.

[36] These differences suggest that a broad range of processes specific to the area where those rocks and soils are observed acted upon them and, therefore, could hold important clues about emplacement mechanisms and post-emplacement modifications that are still debated in many cases. These morphological and sedimentological differences are not reflected in the existing classifications.

[37] There is, therefore, a need for a sedimentological characterization to complete our understanding of the range of geological and morphological processes that took place, first at Gusev and Meridiani, but at any other Martian sites that will be explored in the future with instruments allowing sedimentological classification. This study on Gusev soils is a first step at providing dimensionless indexes to obtain

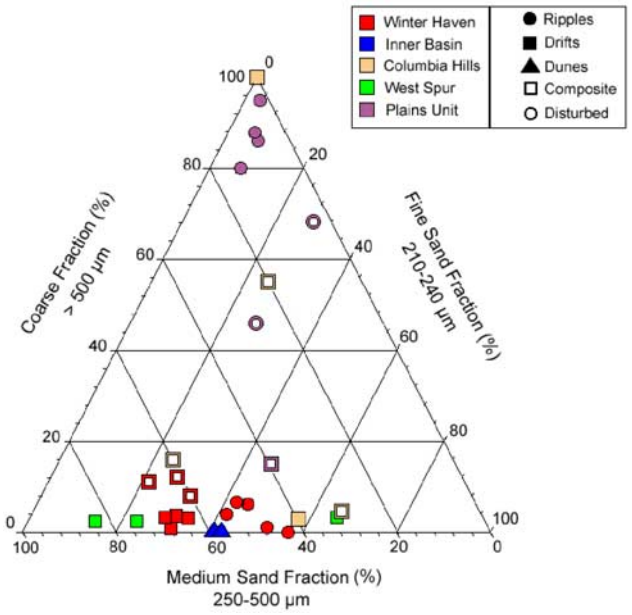

Figure 11. Textural classification of Gusev Soils. For terrestrial soils, textural classification is established on the basis of the respective amounts of silt, clay, and sand in a sample. At MI resolution, silt and clay are not accessible for Martian soils. As a result, textural classification was established using the most characteristic sedimentological fractions. The dune and drifts in Winter Haven are similar sedimentologically. The ripples are coarser on average. All ripples in the Plains Unit show comparable composition. Some soils on Husband Hill have sizes similar to those on the plains but their particle shapes contrast significantly (angular on Husband Hill and rounded on the plains).

such integrated and quantified classification of Martian soils and rocks.

[38] **Acknowledgments.** This work was performed for the Jet Propulsion Laboratory, California Institute of Technology, sponsored by the National Aeronautics and Space Administration Mars Exploration Rover mission. The authors wish to thank the two anonymous reviewers for their helpful comments and suggestions.

References

Alshibli, K. A., and M. I. Alsaleh (2004), Characterizing the roughness and shape of sands using digital microscopy, *J. Comput. Civ. Eng.*, *18*(1), 36–45, doi:10.1061/(ASCE)0887-3801(2004)18:1(36).

Blaney, D. L., P. Christensen, S. Ruff, and the Athena Science Team (2006), Minealogical units in the Columbia Hills from Mini-TES, *Lunar Planet. Sci. Conf., 37th*, Abstract 2057.

Cabrol, N. A., and E. A. Grin (2006), Conditions for aqueous processes in Gusev Crater along the Spirit traverse from the MI and Pancam imagers, paper presented at Mars Water Workshop, NASA Ames, Moffett Field, Calif., 23–24 Feb.

Cabrol, N. A., R. Greeley, and the Athena Science Team (2005), Characterization of non-organized soils at Gusev Crater with the Spirit rover data, *Lunar Planet. Sci. Conf.*, *36*, Abstract 2328.

Cabrol, N. A., J. D. Farmer, E. A. Grin, L. Richter, L. Soderblom, R. Li, K. Herkenhoff, G. A. Landis, and R. E. Arvidson (2006), Aqueous processes at Gusev Crater inferred from physical properties of rocks and soils along the Spirit traverse, *J. Geophys. Res.*, *111*, E02S20, doi:10.1029/2005JE002490.

Cabrol, N. A., E. A. Grin, K. Herkenhoff, L. Richter, and the Athena Science Team (2007), Soil sedimentology, textures and dynamics at Gusev Crater from Spirit's Microscopic Imager, *Lunar Planet. Sci. Conf.*, *38*, Abstract 1784.

Christensen, P. R., et al. (2004), Initial results from the Mini-TES experiment in Gusev Crater from the Spirit rover, *Science*, *305*, 837–842, doi:10.1126/science.1100564.

Dreibus, G., J. Brückner, and R. Gellert, and the Athena Science Team (2006), Chemical composition of rocks in the Columbia Hills at Gusev Crater, Mars, *EPS Conference*, Eur. Phys. Soc., Rome.

Ennis, M. E., M. E. Schmidt, T. McCoy, W. Farrand, and N. A. Cabrol (2007), Hydrovolcano on Mars? A comparison of Home Plate, Gusev Crater and Zuni salt lake maar, New Mexico, *Lunar Planet. Sci. Conf.*, *38*, Abstract 1966.

Gellert, R., et al. (2004), Chemistry of rocks and soils in Gusev Crater from the Alpha Particle X-ray Spectrometer, *Science*, *30*, 829–832, doi:10.1126/science.1099913.

Gellert, R., et al. (2006), Alpha Particle X-Ray Spectrometer (APXS): Results from Gusev crater and calibration report, *J. Geophys. Res.*, *111*, E02S05, doi:10.1029/2005JE002555.

Greeley, R., et al. (2004), Gusev Crater, Mars: Wind-related features and processes at the MER Spirit Site, *Science*, *305*, 810–813, doi:10.1126/science.1100108.

Greeley, R., et al. (2006), Gusev Crater: Wind-related features and processes observed by the Mars Exploration Rover Spirit, *J. Geophys. Res.*, *111*, E02S09, doi:10.1029/2005JE002491.

Greeley, R., et al. (2008), Influence of the topography of the Hills on the orientation of bedforms, *J. Geophys. Res.*, *113*, E06S06, doi:10.1029/2007JE002971.

Haskin, L. A., et al. (2005), Water alteration of rocks and soils on Mars at the Spirit rover site in Gusev Crater, *Nature*, *436*, 66–69, doi:10.1038/nature03640.

Heiken, G., D. Vaniman, and B. M. French (Eds.) (1991), *Lunar Sourcebook: A User's Guide to the Moon*, 736 pp., Cambridge Univ. Press, New York.

Herkenhoff, K. E., et al. (2004), Textures of soils and rocks at Gusev Crater from Spirit's microscopic imager, *Science*, *305*, 824–826, doi:10.1126/science.3050824.

Herkenhoff, K. E., et al. (2006), Overview of the Microscopic Imager Investigation during Spirit's first 450 sols in Gusev Crater, *J. Geophys. Res.*, *111*, E02S04, doi:10.1029/2005JE002574.

Janoo, V. C. (1998), Quantification of shape, angularity, and surface texture of base course materials, *CRREL Spec. Rep. 98-1*, 22 pp., Cold Reg. Res. and Eng. Lab., Hanover, N. H.

McSween, H., et al. (2004), Basaltic rocks analyzed by the Spirit rover at Gusev Crater, *Science*, *305*, 842–845, doi:10.1126/science.3050842.

Ming, D. W., et al. (2006), Geochemical and Mineralogical Indicators for Aqueous Processes in the Columbia Hills of Gusev Crater, Mars, *J. Geophys. Res.*, *111*, E02S12, doi:10.1029/2005JE002560.

Morris, R. V., et al. (2004), Mineralogy at Gusev Crater from the Mössbauer spectrometer on the Spirit rover, *Science*, *305*, 833–836, doi:10.1126/science.1100020.

Morris, R. V., et al. (2006), Mössbauer mineralogy of rock, soil, and dust at Gusev Crater, Mars: Spirit's journey through weakly altered olivine basalt on the plains and pervasively altered basalt in the Columbia Hills, *J. Geophys. Res.*, *111*, E02S13, doi:10.1029/2005JE002584.

Podczeck, F. (1997), A shape factor to assess the shape of particles using image analysis, *Powder Technol.*, *93*(1), 47–53, doi:10.1016/S0032-5910(97)03257-9.

Rice, J. W. Jr., W. Farrand, T. McCoy, M. Schmidt, R. A. Yingst, and the Athena Science Team (2006), Origin of Home Plate, Columbia Hills, Mars: Hydrovolcanic hypothesis, *Eos Trans. AGU*, *87*(52), *Fall Meet. Suppl.*, Abstract P41B-1274.

Rice, J. W. Jr., N. A. Cabrol, T. McCoy, M. Schmidt, S. W. Squyres, and R. A. Yingst (2007), The phreomagmatic origin of Home Plate, Gusev Crater, paper presented at Volcano-Ice Interaction Conference, Univ. of B. C., Vancouver, Canada.

Roedder, E., and P. W. Weiblen (1973), Apollo 17 "orange soil" and meteorite impact on liquid lava, *Nature*, *244*, 210–212, doi:10.1038/244210a0.

Seelos, K., and F. Sirocko (2005), RADIUS—Rapid particle analysis of digital images by ultra-high-resolution scanning of thin sections, *Sedimentology*, *52*(3), 669–681, doi:10.1111/j.1365-3091.2005.00715.x.

Soderblom, L. A., et al. (2004), Soils at the Eagle crater and Meridiani Planum at the Opportunity landing site, *Science*, *306*, 1723–1726, doi:10.1126/science.1105127.

Squyres, S. W., et al. (2006), The rocks of the Columbia Hills, *J. Geophys. Res.*, *111*, E02S11, doi:10.1029/2005JE002562.

Squyres, S. W., et al. (2007), Pyroclastic activity at Home Plate in Gusev Crater, Mars, *Science*, *316*(5825), 738–742, doi:10.1126/science.1139045.

Sullivan, R., et al. (2005), Aeolian processes at the Mars Exploration Rover Meridiani Planum landing site, *Nature*, *436*, 58–61, doi:10.1038/nature03641.

Uthus, L., I. Hoff, and I. Horvli (2005), Evaluation of grain shape characterization methods for urban aggregates, paper presented at 7th International Conference on the Bearing Capacity of Roads, Railways and Airfields, Nor. Univ. of Sci. and Technol., Trondheim, Norway.

Wagner, J. L., G. W. Thomas, and J. Glasgow (2003), Assessing geologic image interpretations errors occurring in extraterrestrial robotic exploration, in *Proceedings of IEEE International Conference on Systems*, *Man and Cybernetics*, vol. 3, pp. 2089–2094, Inst. of Electr. and Electron. Eng., New York.

Wang, A. L., et al. (2006), Sulfate deposition in subsurface regolith in Gusev Crater, Mars, *J. Geophys. Res.*, *111*, E02S17, doi:10.1029/2005JE002513.

Weitz, C. M., et al. (2006), Soil grain analyses at Meridiani Planum, Mars, *J. Geophys. Res.*, *111*, E12S04, doi:10.1029/2005JE002541.

Wilson, L., and J. W. Head III (2007), Dispersal of tephra in explosive eruptions on Mars (1): Stable convecting eruption clouds, *Lunar Planet. Sci. Conf.*, *38*, Abstract 1117.

Yen, A. S., et al. (2005), An integrated view of the chemistry and mineralogy of Martian soils, *Nature*, *436*, 49–54, doi:10.1038/nature03637.

R. C. Anderson, Jet Propulsion Laboratory, M/S 264-422, 4800 Oak Grove Drive, Pasadena, CA 91109, USA.

N. A. Cabrol, E. A. Grin, and J. Moore, NASA Ames Research Center, Space Science and Astrobiology Division, MS 245-3, Moffett Field, CA 94035-1000, USA.

B. A. Cohen, Department of Earth and Planetary Sciences, Northrop Hall, MSCO3-2040, University of New Mexico, Albuquerque, NM 87131-0001, USA.

C. d'Uston, Centre d'Etude Spatiale des Rayonnements 9, Avenue du Colonel Roche, F-31028, Toulouse Cedex 4, France.

B. Franklin, Jet Propulsion Laboratory, M/S 183-501, 4800 Oak Grove Drive, Pasadena, CA 91109, USA.

R. Greeley and A. Knudson, Department of Geological Sciences, Arizona State University, Tempe, AZ 85287-1404, USA.

K. E. Herkenhoff, U.S. Geological Survey, 2255 North Gemini Drive, Flagstaff, AZ 86001, USA.

R. Li, CEEGS/Center for Mapping, Ohio State University, 470 Hitchcock Hall, 2070 Neil Ave., Columbus, OH 43210, USA.

C. Schröder, Institute Inorganic and Analytical Chemistry, Johannes Gutenberg-University, Staudinger Weg 9, D-55099 Mainz, Germany.

C. Weitz, Planetary Science Institute, 1700 E. Fort Lowell Road, Suite 106, Tucson, AZ 85719, USA.

R. A. Yingst, Natural and Applied Sciences, University of Wisconsin Green Bay, Green Bay, WI 54311, USA.